

Benchmarking Cross-Domain Audio-Visual Deception Detection

Xiaobao Guo, Zitong Yu, *Member, IEEE*, Nithish Muthuchamy Selvaraj, Bingquan Shen, Adams Wai-Kin Kong, *Member, IEEE* and Alex C. Kot, *Life Fellow, IEEE*

Abstract—Automated deception detection is crucial for assisting humans in accurately assessing truthfulness and identifying deceptive behavior. Conventional contact-based techniques, like polygraph devices, rely on physiological signals to determine the authenticity of an individual’s statements. Nevertheless, recent developments in automated deception detection have demonstrated that multimodal features derived from both audio and video modalities may outperform human observers on publicly available datasets. Despite these positive findings, the generalizability of existing audio-visual deception detection approaches across different scenarios remains largely unexplored. To close this gap, we present the first cross-domain audio-visual deception detection benchmark, that enables us to assess how well these methods generalize for use in real-world scenarios. We used widely adopted audio and visual features and different architectures for benchmarking, comparing single-to-single and multi-to-single domain generalization performance. To further exploit the impacts using data from multiple source domains for training, we investigate three types of domain sampling strategies, including domain-simultaneous, domain-alternating, and domain-by-domain for multi-to-single domain generalization evaluation. Furthermore, we proposed the Attention-Mixer fusion method to improve performance, and we believe that this new cross-domain benchmark will facilitate future research in audio-visual deception detection. Protocols and source code are available at https://github.com/Redaimao/cross_domain_DD.

Index Terms—audio-visual, multimodal deception detection, cross-domain, generalization.

1 INTRODUCTION

AUDIO-visual deception detection involves utilizing AI techniques and algorithms to automatically detect deceptive behavior in speech and facial movements [5], [6], [7], [8]. Deception detection has a significant impact on various real-world applications such as law enforcement [9], healthcare [10], and business [11]. It has the potential to prevent fraud, improve security measures, and enhance trust and confidence. A reliable deception detection tool can support more accurate decision-makings.

Traditional deception detection is often a contact-based method. It assesses whether someone is telling the truth or not by monitoring physiological responses like skin conductance and heart rate [12]. Experts’ Behavioral observation and analysis are another technique that evaluates changes in a person’s body language, speech patterns, and eye movements [13], [14]. However, such an assessment can be time-consuming and require significant expertise to perform accurately.

Recently, the development of automated deception detection systems using AI and machine learning techniques has gained significant attention as the existing methods have limitations in terms of reliability, accuracy, and scalability.

Manuscript received July, 2023. Corresponding author: Zitong Yu.

- X. Guo is with ROSE Lab, Interdisciplinary Graduate Programme, and also with SCSE, Nanyang Technological University, Singapore. E-mail: xiaobao001@ntu.edu.sg
- Z. Yu, N. M. Selvaraj, and A. Kot are with ROSE Lab, Nanyang Technological University, Singapore. E-mail: zitong.yu@ieee.org, {ms.nithish, eackot}@ntu.edu.sg
- B. Shen is with DSO National Laboratories, Singapore. E-mail: sbingqua@dso.org.sg
- A. W. -K. Kong is with SCSE, Nanyang Technological University, Singapore. E-mail: adamskong@ntu.edu.sg

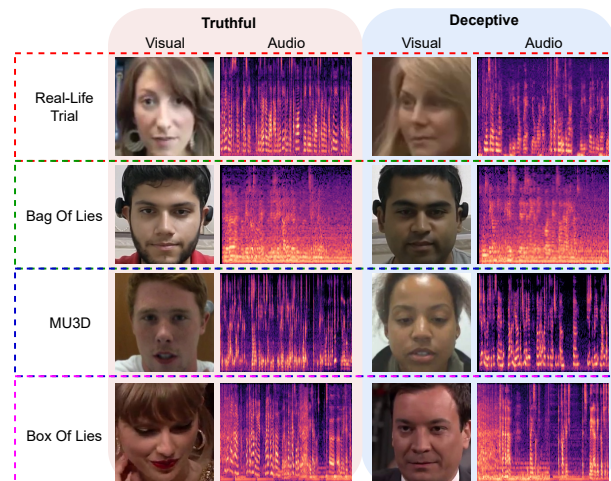


Fig. 1: Typical samples from different publicly deception detection datasets: Real Life Trials [1], Bag of Lies [2], MU3D [3], and Box of Lies [4]. The samples in each row are from different datasets while those in each column are with different modalities (visual vs. audio) and ground truth labels (i.e., truthful vs. deceptive). It can be seen that serious domain shifts (e.g., resolution/illumination/pose in visual faces and pitch/loudness/noise in audio) occur among these datasets.

Various multimodal datasets have been introduced, including real-life trials from court scenes [1], lab-based setups [2], [3], and game show scenarios [4]. These datasets provide a wide variety of deceptive samples from different domains, enabling researchers to examine the effectiveness of AI models on deception detection. Based on these datasets, progress has been made in deception detection techniques

within specific domains [6], [7], [15]. Recent studies have utilized rich visual and audio features [16], [17], [18], such as Mel Spectrogram, emotional states, and facial action units, to enhance the performance of deception detection tasks.

However, there remains a substantial research gap that needs to be addressed. Specifically, fewer studies have explored the cross-domain issue, despite the presence of significant domain shifts in public deception detection datasets. As shown in Figure 1, domain shifts are observed in both audio and visual modalities from publicly available datasets. The generalizability of the models is critical for practical applications. Therefore, such domain shifts need to be investigated in order to develop deception detection models that can be generalized across different contexts. Additionally, effective methods must be proposed to alleviate the domain shift issue by fusing both audio and visual features in a meaningful way. Addressing these issues can benefit automated deception detection systems in improving generalizability in real-world applications.

To address the issue of cross-domain deception detection, we introduce a new benchmark that evaluates the generalization capacity of AI models using audio and visual features over publicly available datasets. Our benchmarking approach utilizes widely adopted audio and visual features, and we compare the single-to-single domain performance and multi-to-single domain generalization using different architectures. Specifically, for the multi-to-single setting, three domain sampling strategies, *i.e.*, domain simultaneous, domain alternating, and domain-by-domain, are implemented to conduct cross-domain testing. To further enhance performance, we propose an Attention-Mixer fusion method based on MLP-Mixer [19]. This benchmarking framework serves as an important tool for evaluating the effectiveness of audio-visual deception detection models in diverse contexts, which will help improve the capabilities of automated deception detection systems in real-world settings. Additionally, we hope our work will inspire further research on multimodal models that address domain shift issues. In summary, our main contributions include:

- Introducing a new benchmark for evaluating the generalization capacity of AI models using audio and visual features across different domains.
- Comparing the single-to-single domain and multi-to-single domain generalization using different architectures.
- Providing three domain sampling strategies *i.e.*, domain simultaneous, domain alternating, and domain-by-domain, to conduct multi-to-single cross-domain testing.
- Proposing the Attention-Mixer fusion method to enhance performance.

In the rest of the paper, Sec. 2 provides a review of related psychological studies on cues to deception and multimodal deception detection works. Sec. 3 introduces our benchmarking approach and fusion method. Sec. 4 provides the cross-domain benchmark results and fusion results. Finally, conclusions and future works are given in Sec. 5.

2 RELATED WORK

2.1 Cues to Deception

The research on using behavioral cues for deception has gradually become active over the past few decades. Psychological researchers have published a large number of works on the analysis of cues to deception [20], [21], [22]. Among the studied behavioral cues, verbal and nonverbal cues were preferred as humans may behave differently between lying and telling the truth. DePaulo *et al.* [23] studied and reported experimental results on 158 cues to deception. They revealed that, in general, people who tell lies are less forthcoming and less convincing than those who tell the truth. Liars usually talk about fewer details and make fewer spontaneous corrections. They also sound less involved but more vocally tense. Through the study, the researchers statistically found that liars often press their lips, repeat words, raise their chins, and show less genuine smiles. The results show that some behavioral cues do potentially appear in deception and are even more pronounced when liars are more motivated to cheat.

Levine *et al.* [24] reviewed the status quo and provided a new perspective on the theories of deception. They pointed out that lying usually happens when problematic information is involved. It is critical to understand the verbal content in the context. Vrij *et al.* [25] realized that interviewers play a vital role in eliciting and enhancing cues to deceit. The authors proposed the “interviewing to detect deception” technique to open a new path in the deception detection research field. They argued that different psychological states can be exploited by adopting appropriate interview techniques of liars and truth-tellers. Hirschberg *et al.* [26] proposed a method to distinguish deceptive from non-deceptive speeches by a large corpus. They also conducted experiments using acoustic, lexical, and speaker-dependent features, which showed improved performance by combining multiple feature sets. Warren *et al.* [27] conducted experiments to investigate the relationship between affective facial expressions to deception. The results indicated that leaked emotions with the incongruous intended message can provide useful cues to deception, which supported the nonverbal leakage theory [28], [29].

2.2 Multimodal Deception Detection

Recent works for deception detection usually use verbal and non-verbal features and propose effective fusion methods [15], [16], [17], [30]. For example, some works utilized facial features from RGB images to perform deception detection [5], [15], [17]. To capture facial movements, facial action units (AUs) were utilized. Other features, such as facial expression, were also adopted [6], [30]. Besides visual features, many works incorporated audio features to boost performance [6], [7], [15]. For example, Wu *et al.* [6] used MFCC (Mel-frequency Cepstral Coefficients) features and Karimi *et al.* [15] used raw audio. Most of the recent works mentioned above have considered multimodal fusion approaches that extract visual, audio, and text information to boost performance. In addition to visual, audio and text, Karnati *et al.* [16] exploited physiological signals, *i.e.*, EEG representations for deception detection.

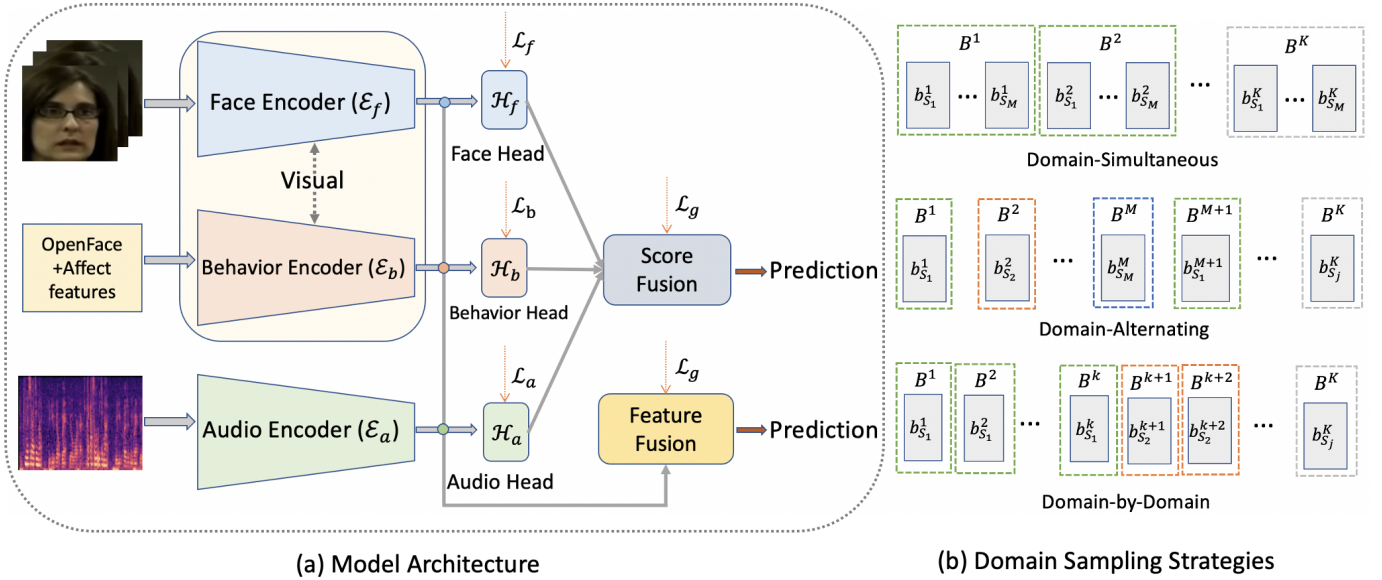


Fig. 2: Main network and method. (a) Model architecture. Visual modality includes face and behavior inputs. Audio modality includes Mel Spectrogram input. The features obtained by the respective encoders. The fusion methods include score fusion and feature fusion. (b) Domain sampling strategies. Domain-simultaneous: each batch consists of samples from multiple sources. Domain-alternating: each batch is alternatively sampled from multiple sources. Domain-by-domain: the batches are sampled from one source and then from another.

To better fuse the multimodal features, different fusion methods were proposed, which can be broadly categorized into feature-level fusion and decision-level fusion. Specifically, feature-level fusion focused on producing better multimodal embeddings and used the linear layers to extract crossmodal dynamics [5], [6], [7], [15], [17]. Rather than that, decision-level fusion aimed to fuse multimodal dynamics at a late stage, to reduce computational complexity and learn good marginal representations [7], [16].

However, previous works on multimodal deception detection did not consider cross-domain issues that occur from one domain to another, which is the focus of this work.

3 METHODOLOGY

The mainstream architecture for audio-visual deception detection usually includes encoders for unimodal feature extraction and/or a fusion module. We follow the widely adopted architecture to build the benchmark on cross-domain audio-visual deception detection in this work. As shown in Fig. 2, audio and visual features are extracted from audio and visual encoders. The fusion module is performed based on audio and visual features. The fused feature is input to the classifier for classification. We build the benchmark for cross-domain generalization performance based on such network architecture with different encoders. We conducted single-to-single and multi-to-single evaluations where three domain sampling strategies included, *i.e.*, domain-simultaneous, domain-alternating, and domain-by-domain.

3.1 Audio and Visual Feature Learning

To establish a benchmark for cross-domain audio-visual deception detection, we utilize widely adopted audio and

visual features along with their respective encoders. Our approach treats audio and visual features as equally important, extracting different types of features simultaneously. As depicted in Fig. 1, this network structure offers several advantages: (1) flexibility in network selection: different audio or visual encoders can be effortlessly incorporated and compared in a fair manner, (2) adaptability: the addition or removal of specific modules and/or losses is straightforward. For instance, a fusion module can be inserted before classifiers, and (3) easy performance benchmarking: the system facilitates evaluating performance in various settings, such as score-level fusion and feature-level fusion. In this work, we focus on audio and visual modalities for deception detection. In particular, two kinds of visual features are extracted, *i.e.*, face features from RGB face images and behavior features consist of AUs, affects, etc.

As shown in Fig. 1, given a detected RGB face image as input X_f , the deep features F_f could be extracted via face encoder networks \mathcal{E}_f (e.g., ResNet18 [31]). Similarly, behavior inputs such as the AU and/or affect features X_b are encoded by OpenFace [32] or affect model (e.g., EmotionNet [33]) \mathcal{E}_b to output behavior features F_b . Note that we regard both face frames and behavior features as the visual modality but differentiate them in this work as they have different types of information and representations. Given audio input X_a (either Mel Spectrogram [34] or waveforms), audio features F_a are extracted through audio encoder \mathcal{E}_a . The corresponding classification heads for face frames (\mathcal{H}_f), behavior features (\mathcal{H}_b), and audio features (\mathcal{H}_a) output the prediction logits \hat{Y}_f , \hat{Y}_b , and \hat{Y}_a , respectively. The fusion head \mathcal{G} takes F_f , F_b , and F_a as input. \mathcal{G} is determined by the actual fusion method, e.g., liner layer, transformer layers, MLP, etc. The output logit of \mathcal{G} is denoted by \hat{Y}_g . Therefore, the audio and visual learning process can be denoted as

follows:

$$\begin{aligned} F_f &= \mathcal{E}_f(X_f), \hat{Y}_f = \mathcal{H}_f(F_f), \\ F_b &= \mathcal{E}_b(X_b), \hat{Y}_b = \mathcal{H}_b(F_b), \\ F_a &= \mathcal{E}_a(X_a), \hat{Y}_a = \mathcal{H}_a(F_a), \\ \hat{Y}_g &= \mathcal{G}(F_f, F_b, F_a). \end{aligned} \quad (1)$$

Loss Function. For deception detection ground truth Y , where $Y = 0$ for truthful and $Y = 1$ for deception, the binary cross-entropy loss (BCE) is adopted. The loss for each sample with a certain modality or fused prediction can be denoted as

$$\mathcal{L}_m = -(Y \log(\hat{Y}_m) + (1 - Y) \log(1 - \hat{Y}_m)), \quad (2)$$

where $m \in \{f, b, a, g\}$, \hat{Y}_m is the corresponding prediction logits. In other words, the BCE loss is calculated separately for each type of modality and/or its fused feature depending on whether a sample has any face frames, visual inputs, or audio inputs. The overall loss function can be described as follows:

$$\mathcal{L} = \frac{1}{N} \sum_{i=1}^N \left(\sum_{m=f,b,a} \mathcal{L}_{m,i} + \lambda \mathcal{L}_{g,i} \right), \quad (3)$$

where N is the number of data samples and λ is a trade-off parameter between modality loss and fusion loss. λ is set to 0.5 in our experiments.

3.2 Cross-domain Generalization

We benchmark the cross-domain generalization on the deception detection task. First, we introduce the notations and definitions in this section. A domain is composed of data that are sampled from a distribution (dataset), which can be denoted as $\mathcal{S} = \{(X; Y)_i\}_{i=1}^N \sim P_S$, where $X = (X_f, X_b, X_a)$, X_f, X_b, X_a represent samples of face frames, behavior, and audio modalities, respectively. Y denotes the label, and P_S denotes the joint distribution of the input samples and the output label. In this paper, for simplicity, we follow similar definitions in [35], [36] to treat each dataset as an individual domain due to their obvious distribution gaps, but more fine-grained intra-domain factors would be explored in future work. For domain generalization, M source domains (training datasets) are given, i.e., $\mathcal{S}_{train} = \{S_j | j = 1, \dots, M\}$, where $S_j = \{(X; Y)_i\}_{i=1}^{N_j} \sim P_{S_j}$ denotes the j -th domain, and $P_{S_i} \neq P_{S_j}$ for $1 \leq i, j \leq M$. N_j is the number of total samples in S_j . The goal of domain generalization is to learn the predictive function h in M source domains to achieve minimum error on an unseen test domain $\mathcal{S}_{test} \sim P_{S_{test}}$, and $P_{S_{test}} \neq P_{S_j}$ for $1 \leq j \leq M$:

$$\min \mathbb{E}_{(X; Y) \in \mathcal{S}_{test}} [\mathcal{L}(h(X), Y)], \quad (4)$$

where $X = (X_f, X_b, X_a)$, Y is the label, \mathcal{L} is the loss function, and \mathbb{E} is the expectation.

When $M = 1$, it is a *Single-to-single Cross-domain Generalization* task, where the model is trained on one training dataset and tested on another dataset. When $M \geq 2$, we propose three strategies to learn from multiple domains for the *Multi-to-single Cross-domain Generalization*. Let B denote one batch of training data with a size of N_B . Given multiple

training domains $\mathcal{S}_{train} = \{S_j | j = 1, \dots, M\}$, B is a set of training data sampled from \mathcal{S}_{train} .

Domain-Simultaneous means to train multiple domains in parallel within each batch of data. In domain simultaneous training, the k -th batch of training data is a group of samples from different domains, i.e., $B^k = (b_{S_1}^k, \dots, b_{S_M}^k)$, $k \in [1, \dots, K]$, where $b_{S_j}^k$ is the batch samples from domain S_j for $j = 1, \dots, M$, K is the number of batches during training. The total number of $b_{S_j}^k$ is N_B . As shown in Fig. 2 (b), each training batch contains smaller batch samples from all the source domains during training. Models are trained to learn from different domains simultaneously by feeding the mixed batch data.

Domain-Alternating is different from domain simultaneous strategy in terms of batch samples. In domain-alternating, $B^k = b_{S_j}^k$ for $j = k - \lfloor \frac{k-1}{M} \rfloor \cdot M$, where $\lfloor \cdot \rfloor$ is the flooring operator. The number of $b_{S_j}^k$ is N_B . Fig. 2 (b) shows that the consecutive batch samples come from different domains.

Domain-by-Domain aims to train the model by feeding data from source domain data one by one. $B^k = b_{S_j}^k$ for $\lceil \frac{\sum_{i=0}^{j-1} N_i}{N_B} \rceil \leq k \leq \lceil \frac{\sum_{i=0}^j N_i}{N_B} \rceil$, $N_0 = 0$, where $\lceil \cdot \rceil$ is the ceiling operator. The number of $b_{S_j}^k$ is N_B . As shown in Fig. 2, the batch data samples from one domain after finishing sampling from its previous domains.

3.3 Attention-Mixer Fusion

Besides investigating cross-domain sampling strategies, inspired by [19], we propose *Attention-Mixer Fusion* to enhance the performance by fusing audio-visual modalities, where the attention mixer layer takes multimodal features as input to produce fused features. In particular, an attention mixer layer is composed of unimodal MLP layers, self-attention layers [37], and crossmodal MLP layers. First, for batch size N_B , the input features from different modalities are concatenated and projected to be a tensor $U \in \mathbb{R}^{N_B \times N_m \times D}$ by a Linear layer, followed by several attention mixer layers, where N_m is the number of input modalities. Specifically, the unimodal MLP layer, the self-attention layer, and the crossmodal MLP layer can be respectively described as

$$U^{*,*,i} = F_g^{*,*,i} + \mathbf{W}_2 \sigma(\mathbf{W}_1 \text{LN}(F_g^{*,*,i})), \quad i = [1, D], \quad (5)$$

$$U = \left[\left[\text{softmax} \left(\frac{U \mathbf{W}_3 (U \mathbf{W}_4)^T}{\sqrt{D}} \right) U \mathbf{W}_5 \right]_h \mathbf{W}_6 \right], \quad h = [1, H], \quad (6)$$

$$U^{*,j,*} = U^{*,j,*} + \mathbf{W}_8 \sigma(\mathbf{W}_7 \text{LN}(U^{*,j,*})), \quad j = [1, N_m], \quad (7)$$

where $\text{LN}(\cdot)$ denotes the Layer Normalization, \mathbf{W}_{1-8} are trainable weights, H is the number of heads in multihead self-attention, and $*$ denotes all the entries in that dimension. Several attention mixer layers are stacked as a deep block, which is set as a hyperparameter in practice. We set it to 6 in our experiment. Finally, $U \in \mathbb{R}^{N_B \times N_m \times D}$ is reduced to $U \in \mathbb{R}^{N_B \times N_m \times 1}$ by obtaining the mean value on the feature dimension. In Eq. 5, the unimodal MLP layer is conducted along the feature dimension to learn the dynamics in each unimodal feature. Eq. 6 shows the multi-head self-attention operation on the tensor U , which further explores the attention between the unimodal features. In Eq. 7, the crossmodal MLP layer learns the dynamics across

the modality dimension from the corresponding feature tokens.

4 EXPERIMENTS

In this part, extensive experiments are conducted to benchmark the cross-domain performances on public deception detection datasets. In the following, we sequentially describe the benchmark datasets & metrics (Sec. 4.1), implementation details (Sec. 4.2), benchmarking results (Sec. 4.3 - 4.4) and fusion performances (Sec. 4.5).

4.1 Databases and Metrics

Datasets. We benchmarked the cross-domain generalization performance based on four publicly available datasets. Real Life Trials [1] dataset is a popular real-world dataset collected from public court trials, which consists of 121 videos including 61 deceptive and 60 truthful video clips. As it is a real-world dataset, the Real Life trial dataset has more noise on both the video and audio. We filtered out some corrupted videos and obtained 108 videos (54 truthful and 54 deceptive) with 58 subjects for our experiments. Bag of Lies [2] is a multimodal dataset collected from well-controlled lab-based scenarios, where video, audio, EEG, and gaze data are collected. It has 35 subjects, 163 truthful and 162 deceptive video clips. The backgrounds for the videos are relatively clean and it is less noisy. MU3D [3] has 320 video clips and 80 subjects that cover different races and genders. It is also a lab-based dataset that uses the personal description paradigm to stimuli real-world cases. Each participant tells a positive truth, a positive lie, a negative truth, and a negative lie. Box of Lies [4] is a deception dataset collected from an online gameshow, which has 25 videos and 26 participants (6 male and 20 female). The full video set contains 29 truthful and 36 deceptive rounds of games. However, the quality of the original Box of Lies dataset is not satisfactory. The visual (the face of the participant) and audio from many clips are not matching due to the frequent changes of viewpoints. To perform a fair comparison, we preprocessed and cleaned the Box of Lies dataset. After preprocessing, 101 video clips were extracted for testing. Some of the typical samples from these datasets are shown in Fig. 1.

Evaluation Metrics. In this work, we followed the widely adopted metric, binary classification accuracy (%), for experimental evaluation. The deceptive clips were labeled as 1 and truthful clips were labeled as 0.

4.2 Implementation Details

Feature Extraction. Several widely-adopted audio and visual features were extracted by different tools. For visual features, OpenFace [32] was used to extract 35-dimensional AUs and 8-dimensional gaze features. Face frames were extracted and aligned by MTCNN [39], where we uniformly sampled 64 face frames for each video clip. Affect features were extracted by Emonet [33], where the feature included 5-class emotions, arousal, and valence. For audio features, Mel Spectrograms were extracted by OpenSmile toolkit [34]. Raw audio waveforms were also used in our experiments.

Protocols. Inspired by [35], [36], we treated each dataset as a domain. To evaluate the models' cross-domain generalization capacity and alleviate domain information leakage, all the preprocessed data including original training and test data from each dataset was used for either training or testing. Note that the Box of Lies dataset was only used for testing as many samples were filtered out due to their unsatisfactory quality. The experiments were conducted on the *single-to-single domain* (e.g., R to B1 stands for training on Real-life Trial (R) and testing on Bag of Lies (B1)) and *multi-to-single domain* (e.g., R&M to B2 stands for training on Real-life Trial (R) and MU3D (M) and testing on Box of Lies (B2)).

Model Selection. Models for audio and visual modalities were selected to fit the data volume. For face frames, we adopted ResNet18 [31] and Gate Recurrent Unit (GRU) [40] models for facial feature extraction and temporal modeling, respectively. Two-layer multilayer perception (MLP) [41] models were used for AUs, gaze, and affect feature representation. For the audio-based Mel spectrogram, we used the ResNet18 [31] model for time-frequency feature representation. For audio waveforms, the Wave2Vec [42] model was applied for audio feature extraction.

Experimental Setting. Our proposed method was implemented with Pytorch. The ImageNet pretrained models (e.g., ResNet18) for classification were trained on the benchmark datasets using SGD optimizer with the initial learning rate (lr), momentum, and weight decay (wd) were 1e-3, 0.9, and 5e-5, respectively. We trained models with a maximum of 30 epochs and batchsize 32 on a single Nvidia V100 GPU. As for the fusion models (e.g., Atten-Mixer on face frames and Mel Spectrogram), Adam optimizer with initial lr=1e-3 and wd=5e-5 was used. The models were trained with batchsize 16 for a maximum of 30 epochs.

4.3 Cross-domain Testing with Unimodal Features

In this subsection, we present the benchmark results of cross-domain testing by investigating unimodal features to evaluate their generalization capacities. For clarity, we use "visual (face frames)" to indicate face inputs and "visual (AU/gaze/affect)" to indicate behavior inputs.

Single-to-Single Domain. Specifically, the models were trained on one dataset from one domain and tested on the other dataset from another domain. The experiments were conducted on the four public datasets, Real-life Trial (R), Bag of Lies (B1), Box of Lies (B2), and MU3D (M). As shown in Tabel 1, for visual modalities, we extracted the most adopted visual features including face frames, and behavior features such as AUs, gaze and affect. For audio modality, Mel spectrogram and waveform were extracted. We also applied several different backbone networks as audio and visual encoders. We can observe that R and B1 datasets generalized the best on B2, and M generalized the best on R. Note that the B2 dataset was not adopted as a source domain dataset as the original dataset had too much noise and we cleaned it only for testing. On average, we can observe that the best result was achieved by using visual (AU+gaze+affect) features.

Multi-to-Single Domain. Here we fully evaluate the performance of multi-to-single cross-domain generalization us-

TABLE 1: The results of single-to-single cross-domain generalization accuracy (%) on benchmark datasets, Real-life Trial (R), Bag of Lies (B1), Box of Lies (B2), and MU3D (M).

Modality & Inputs	Method	R to B1	R to B2	R to M	B1 to R	B1 to B2	B1 to M	M to R	M to B1	M to B2	Avg
Visual (AU)	LSTM [38]	48.11	-	-	61.21	-	-	-	-	-	-
Visual (Face frames)	ResNet18	52.00	61.39	51.25	50.93	57.43	50.62	57.94	51.69	57.43	54.52
Visual (Face frames)	ResNet18+GRU	53.54	63.37	52.81	57.41	59.41	51.56	46.73	52.92	55.45	54.80
Visual (AU+Gaze)	MLP	50.77	65.35	56.87	58.88	58.42	50.94	46.73	51.69	53.47	54.79
Visual (Affect)	MLP	50.46	58.42	50.31	50.47	51.49	52.19	66.36	51.08	60.40	54.58
Visual (AU+Gaze+Affect)	MLP	54.46	59.41	54.37	50.47	57.43	54.69	60.75	51.69	55.45	55.41
Audio (Mel spectrogram)	ResNet18	46.77	53.47	52.19	50.47	66.34	50.62	54.21	51.38	55.45	53.43
Audio (Waveform)	Wave2Vec	51.08	48.51	50.94	46.73	58.42	50.00	63.55	56.31	56.44	53.55

TABLE 2: The results of multi-to-single cross-domain generalization accuracy (%) on benchmark datasets, Real-life Trial (R), Bag of Lies (B1), Box of Lies (B2), and MU3D (M), for different generalization strategies.

Modality & Inputs	Method	R&M to B1	R&M to B2	R&B1 to B2	R&B1 to M	B1&M to R	B1&M to B2	R&B1&M to B2	Avg
Domain-Simultaneous									
Visual (Face frames)	ResNet18	53.85	49.50	49.50	50.94	44.86	60.40	44.55	50.51
Visual (Face frames)	ResNet18+GRU	52.62	54.46	51.49	51.88	53.27	59.41	44.55	52.53
Visual (AU+Gaze)	MLP	53.54	47.52	48.51	50.94	52.34	53.47	56.44	51.82
Visual (Affect)	MLP	50.15	54.46	55.45	52.19	53.27	57.43	62.38	55.04
Visual (AU+Gaze+Affect)	MLP	50.46	52.48	61.39	51.25	51.4	60.4	63.37	55.82
Audio (Mel spectrogram)	ResNet18	48.92	45.54	53.47	53.12	43.93	62.38	50.5	51.12
Audio (Waveform)	Wave2Vec	52.92	55.45	44.55	51.25	69.16	42.57	46.53	51.78
Domain-Alternating									
Visual (Face frames)	ResNet18	50.15	45.54	56.44	51.56	50.47	54.46	65.85	53.50
Visual (Face frames)	ResNet18+GRU	55.38	52.48	60.40	50.00	50.47	60.40	64.62	56.25
Visual (AU+Gaze)	MLP	55.45	47.52	53.47	51.25	54.21	57.43	60.40	54.25
Visual (Affect)	MLP	51.08	56.44	61.39	52.19	52.34	58.42	53.47	55.05
Visual (AU+Gaze+Affect)	MLP	51.38	58.42	63.37	50.31	53.27	52.48	60.40	55.66
Audio (Mel spectrogram)	ResNet18	50.15	60.40	53.47	50.31	58.88	51.49	47.52	53.17
Audio (Waveform)	Wave2Vec	52.92	55.45	44.55	50.62	64.49	58.42	48.51	53.57
Domain-by-Domain									
Visual (Face frames)	ResNet18	52.00	53.47	56.44	50.00	59.81	41.58	55.45	52.68
Visual (Face frames)	ResNet18+GRU	54.46	41.58	66.34	50.62	51.40	56.44	60.40	54.46
Visual (AU+Gaze)	MLP	51.08	43.56	55.45	53.75	57.01	53.47	54.46	52.68
Visual (Affect)	MLP	55.69	57.43	57.43	51.56	52.34	49.50	61.39	55.05
Visual (AU+Gaze+Affect)	MLP	50.15	56.44	58.42	50.00	57.94	60.40	63.37	56.67
Audio (Mel spectrogram)	ResNet18	52.31	50.50	58.42	49.38	53.27	56.44	59.41	54.24
Audio (Waveform)	Wave2Vec	56.00	47.52	44.55	53.12	67.29	57.43	58.42	54.90

ing unimodal features. We conducted experiments for different domain sampling strategies. As shown in Table 2, for domain-simultaneous training, the best generalization performance is achieved by training on the Bag of Lies and MU3D datasets and testing on the Real-life Trial dataset (69.16%), which was also the case for domain-by-domain training strategy (67.29%). For the domain-alternating strategy, the best result was observed when transferring to the Box of Lies dataset using the rest three datasets for training (65.85%). The results showed that the best generalization performances were obtained when transferring to the real-world dataset and the gameshow dataset by training on the lab-based datasets. This was because the lab-based datasets (Bag of Lies and MU3D) are relatively clean compared to the real-world dataset (Real-life Trial) and the gameshow dataset (Box of Lies). However, in the opposite case, the generalization performance degraded, for example, R&M to B1 and R&B1 to M. Different domain sampling strategies reached their best average performance on different input features and backbone networks. To be specific, for both domain-simultaneous and domain-by-domain strategies, models trained on visual (AU+gaze+affect) features reached their highest accuracies, which were 55.82% and 56.67%, respectively. Using the domain-alternating strategy, the best accuracy of 56.25% was achieved by training on visual (face frames) features. We can observe that models trained on visual modalities outperformed those trained on audio modalities across all the generalization strategies. This

may be due to the rich deceptive cues captured by visual modalities in the publicly available datasets.

4.4 Domain-Simultaneous with Gradient Reversal Layer (GRL)

Following the implementation by Ganin *et al.* [43], we compared the multi-to-single domain generalization accuracies w/w.o GRL. GRL was proposed to mitigate the domain shift issue by manipulating the training gradients. It worked by acting as an identity transform in forward propagation and multiplying the gradient by a certain negative constant during the backpropagation without having trainable parameters. GRL was inserted between encoders and domain classifiers, which was easy to implement. As GRL is a widely adopted method for domain generalization, it is investigated to show its effectiveness for the deception detection task. We selected domain-simultaneous as the baseline and added GRL to the original network with the same training setups. The average accuracies were reported in Fig. 3, where different types of visual and audio features and methods were compared. Training with GRL, the performance of ResNet18 and ResNet18+GRU models using visual (face frames) features and Wave2Vec model using waveform were enhanced. However, we observed that MLP models using visual (AU/gaze/affect) features and the ResNet18 model using Mel spectrograms degraded in performance. Generally, ResNet18 trained with GRL performed better than MLP for visual modality, and Wave2Vec

TABLE 3: The fusion results of single-to-single cross-domain generalization accuracy (%).

Modality & Inputs	Fusion Position	Fusion Method	R to B1	R to B2	R to M	B1 to R	B1 to B2	B1 to M	M to R	M to B1	M to B2	Avg
Visual (Face frames) + Visual (AU+Gaze+Affect)	Score-level	Average	53.23	41.58	51.88	64.49	62.38	50.62	57.94	53.23	62.38	55.30
		Concat	51.08	55.45	51.88	54.21	58.42	51.25	57.01	50.15	61.39	54.54
	Feature-level	SE-Concat	53.85	60.40	51.25	55.14	58.42	50.62	56.07	51.38	65.35	55.83
		Cross-Atten	55.38	61.39	52.19	51.40	60.40	51.25	55.14	56.31	60.40	55.98
		MLP-Mixer	55.08	48.51	53.44	56.07	58.42	53.75	55.14	59.08	59.41	55.43
		Atten-Mixer(Ours)	56.92	59.41	57.94	63.37	53.75	53.75	60.75	56.00	61.39	58.14
Visual (Face frames) + Audio (Mel spectrogram)	Score-level	Average	53.23	49.50	51.88	50.47	59.41	53.75	65.42	56.31	49.50	54.39
		Concat	50.77	53.47	50.47	62.38	51.56	51.88	54.21	52.62	58.42	53.98
	Feature-level	SE-Concat	50.15	44.55	51.40	61.39	53.12	52.50	65.42	56.31	66.34	55.69
		Cross-Atten	54.46	51.49	55.14	58.42	51.25	52.19	63.55	56.62	66.34	55.95
		MLP-Mixer	52.31	55.45	57.94	63.37	53.12	51.25	64.49	57.85	62.38	57.57
		Atten-Mixer(Ours)	57.54	55.45	56.07	61.39	50.94	53.12	67.29	57.85	64.36	58.22
Visual (AU+Gaze+Affect) + Audio (Mel spectrogram)	Score-level	Average	49.85	58.42	54.06	45.79	60.40	50.62	49.53	56.00	63.37	54.23
		Concat	49.54	53.47	47.66	61.39	53.44	51.88	57.01	50.15	58.42	53.66
	Feature-level	SE-Concat	50.15	48.51	55.14	60.40	53.12	50.00	57.01	49.85	63.37	54.17
		Cross-Atten	53.23	44.55	57.94	55.45	54.69	54.06	63.55	51.69	64.36	55.50
		MLP-Mixer	49.54	57.43	50.47	63.37	54.06	53.12	59.81	55.08	69.31	56.91
		Atten-Mixer(Ours)	53.52	54.46	57.94	61.39	53.12	51.56	69.16	58.15	64.36	58.18
Visual (Face frames) + Visual (AU+Gaze+Affect) + Audio (Mel spectrogram)	Score-level	Average	52.00	58.42	51.88	53.27	58.42	50.94	57.01	53.54	61.39	55.20
		Concat	53.23	58.42	55.14	61.39	52.50	52.19	56.07	54.15	60.40	55.94
	Feature-level	SE-Concat	51.38	58.42	51.40	62.38	52.81	50.94	59.81	54.77	52.48	54.93
		Cross-Atten	51.08	48.51	55.14	60.40	53.12	53.44	60.75	56.31	60.40	55.46
		MLP-Mixer	55.69	46.53	44.86	63.37	51.56	50.94	64.49	56.00	60.40	54.87
		Atten-Mixer(Ours)	55.08	60.40	57.01	64.36	53.44	51.25	67.29	56.00	62.38	58.58

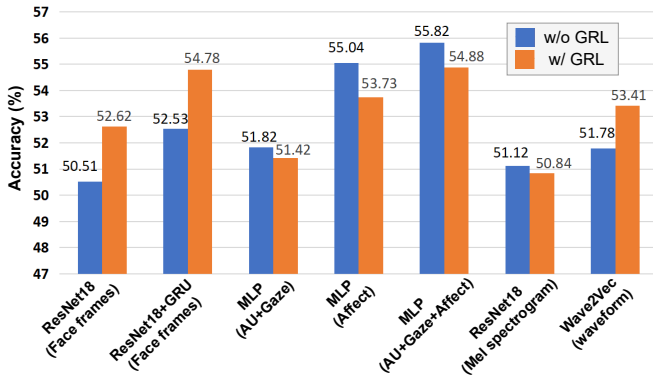


Fig. 3: Performance comparisons of Domain-simultaneous training w/ and w/o Gradient Reversal Layer (GRL).

trained with GRL boosted the performance and surpassed the model trained on the Mel spectrogram.

4.5 Cross-domain Testing with Multimodal Fusion

Here we present multimodal fusion results of cross-domain testing to evaluate models' generalization capacities.

Single-to-Single Domain with Fusion. In this section, we conducted experiments of single-to-single cross-domain testing. Two types of fusion positions were involved including score-level and feature-level fusion. For feature-level fusion, multiple fusion methods were adopted such as simple concatenation, SE-Concat [44], Cross-Atten [37], MLP-Mixer [19], and Attention-Mixer fusion (Ours). To be specific, simple concatenation refers to the concatenation of the extracted features before the input to the classifier. SE-concat stands for the SE attention applied to the concatenated features. Cross-Atten means the crossmodal attention among input features by using the attention mechanism from the Transformer. MLP-Mixer uses the method in [19] on the extracted features. The modalities and input include three types, visual (face frames), visual (AU+gaze+affect), and audio (Mel spectrogram). It results in four combinations of either two or three types of inputs. As shown in

Table 4, among each type of input combination, the proposed Attention-Mixer fusion (Atten-Mixer) achieved the best results. The rest fusion methods showed comparable results, which were less performed than Atten-Mixer.

Multi-to-Single Domain with Fusion. We benchmarked multi-to-single cross-domain generalization with different fusion methods by three types of cross-testing strategies. In total, seven sub-experiments were conducted for different domain combinations. The results are shown in Table 4. On average, the best accuracies were 58.43%, 59.13%, and 60.78% on domain-simultaneous, domain-alternating, and domain-by-domain strategies, respectively. Among these, for both domain-simultaneous and domain-by-domain strategies, the best results were achieved by taking visual (face frames) and visual (AU+gaze+affect) features as input, while the best result for domain-alternating was achieved by using visual (face frames), visual (AU+gaze+affect) and audio (Mel spectrogram) features. Taking a close look at the average fusion results, for each type of modality input, Atten-Mixer achieved the best among the six fusion methods, showing the effectiveness of the proposed method. By using Atten-Mixer, in general, the average result showed slightly better when using the domain-by-domain strategy and taking visual (face frames) and visual (AU+gaze+affect) features as input. To sum up, the results showed that on the current publicly available datasets, visual features were better when it came to multi-to-single cross-domain generalizability. However, the performance differences were not a large gap, and there were also no significant differences by comparing two-to-one domain and three-to-one domain cross-testing performances.

Ablation Study for Attention-Mixer Fusion Module. We conducted an ablation study for the proposed attention-mixer fusion module with the changes in the number of attention-mixer layers. The experiments were conducted on single-to-single domain testing, where the average accuracies were compared. As shown in Fig. 4, the number of attention-mixer layers was set to 4, 5, 6, and 7. The modalities and inputs in Table 3 are compared, where "A" had the inputs of Visual (Face frame) + Visual(AU+Gaze+Affect), "B" had Visual (Face frames) + Au-

TABLE 4: The fusion results of multi-to-single cross-domain generalization accuracy (%) for different generalization strategies.

Modality & Inputs	Fusion Postion	Fusion Method	R&M to B1	R&M to B2	R&B1 to B2	R&B1 to M	B1&M to R	B1&M to B2	R&B1&M to B2	Avg
Domain-Simultaneous										
Visual (Face frames) + Visual (AU+Gaze+Affect)	Score-level	Average	53.23	43.56	57.43	50.94	51.40	58.42	48.51	51.93
		Concat	52.00	56.44	60.40	51.88	51.40	62.38	57.43	55.99
	Feature-level	SE-Concat	55.69	58.42	44.55	52.50	56.07	58.42	58.42	54.87
		Cross-Atten	51.08	52.48	55.45	51.56	57.01	60.40	57.43	55.06
		MLP-Mixer	53.85	43.56	62.38	52.19	56.07	61.39	59.41	55.55
		Atten-Mixer(Ours)	53.23	57.43	63.37	52.19	57.01	63.37	62.38	58.43
Score-level	Average	49.54	55.45	52.48	51.25	54.21	59.41	55.45	53.97	
	Concat	49.54	54.46	49.50	53.75	44.86	63.37	54.46	52.85	
Visual (Face frames) + Audio (Mel spectrogram)	Feature-level	SE-Concat	52.00	58.42	42.57	51.56	54.21	58.42	63.37	54.36
		Cross-Atten	50.46	52.48	60.40	53.12	52.34	58.42	59.41	55.23
	MLP-Mixer	53.54	57.43	52.48	50.31	52.34	60.40	47.52	53.43	
	Atten-Mixer(Ours)	55.69	64.36	56.44	53.75	58.88	59.41	58.42	58.14	
Visual (AU+Gaze+Affect) + Audio (Mel spectrogram)	Score-level	Average	48.62	58.42	56.44	50.94	51.40	56.44	53.47	53.68
		Concat	48.31	53.47	56.44	50.31	56.07	63.37	57.43	55.06
	Feature-level	SE-Concat	49.85	50.50	47.52	52.19	49.53	57.43	61.39	52.63
		Cross-Atten	51.38	63.37	61.39	51.25	48.60	59.41	58.42	56.26
		MLP-Mixer	55.69	59.41	57.43	53.75	50.47	61.39	50.50	55.52
		Atten-Mixer(Ours)	55.08	55.45	58.42	54.37	52.34	61.39	60.40	56.78
Score-level	Average	54.77	57.43	57.43	52.81	60.75	58.42	56.44	56.86	
	Concat	54.46	54.46	47.52	53.12	53.27	61.39	56.44	54.38	
Visual (AU+Gaze+Affect) + Audio (Mel spectrogram)	Feature-level	SE-Concat	53.23	55.45	54.46	52.50	59.81	56.44	58.42	55.76
		Cross-Atten	48.62	57.43	50.50	53.12	48.60	58.42	56.44	53.30
	MLP-Mixer	48.92	48.51	59.41	52.81	54.21	57.43	51.49	53.25	
	Atten-Mixer(Ours)	52.31	59.41	58.42	52.50	58.88	61.39	60.40	57.62	
Domain-Alternating										
Visual (Face frames) + Visual (AU+Gaze+Affect)	Score-level	Average	55.38	57.43	58.42	50.94	57.94	50.50	61.39	56.00
		Concat	55.08	58.42	63.37	51.56	62.62	62.38	53.47	58.13
	Feature-level	SE-Concat	50.46	49.50	63.37	52.19	57.01	65.35	56.44	56.33
		Cross-Atten	55.08	59.41	60.40	52.50	48.60	58.42	61.39	56.54
		MLP-Mixer	57.54	63.37	63.37	50.94	65.42	52.48	56.44	58.51
		Atten-Mixer(Ours)	56.62	61.39	63.37	51.56	58.88	62.38	58.42	58.95
Visual (Face frames) + Audio (Mel spectrogram)	Score-level	Average	50.15	58.42	60.40	50.62	51.40	60.40	58.42	55.69
		Concat	53.23	62.38	54.46	51.25	59.81	54.46	54.46	55.72
	Feature-level	SE-Concat	50.15	52.48	64.36	50.31	59.81	55.45	50.50	54.72
		Cross-Atten	52.92	57.43	49.50	52.81	65.42	53.47	66.34	56.84
		MLP-Mixer	51.69	58.42	57.43	51.25	62.62	58.42	56.44	56.61
		Atten-Mixer(Ours)	53.23	63.37	56.44	51.25	63.55	59.41	56.44	57.67
Visual (AU+Gaze+Affect) + Audio (Mel spectrogram)	Score-level	Average	51.38	56.44	54.46	50.00	64.49	61.39	49.50	55.38
		Concat	49.85	62.38	58.42	51.88	61.68	55.45	51.49	55.88
	Feature-level	SE-Concat	50.46	62.38	58.42	50.00	57.94	59.41	65.35	57.71
		Cross-Atten	49.85	62.38	50.50	53.44	58.88	56.44	56.44	55.42
		MLP-Mixer	50.15	55.45	58.42	50.31	58.88	61.39	57.43	56.00
		Atten-Mixer(Ours)	50.15	59.41	50.50	52.19	58.88	60.40	61.39	56.13
Visual (Face frames) + Visual (AU+Gaze+Affect) + Audio (Mel spectrogram)	Score-level	Average	56.00	52.48	59.41	51.88	51.40	60.40	56.44	55.43
		Concat	51.69	58.42	58.42	52.81	57.01	61.39	56.44	56.60
	Feature-level	SE-Concat	56.31	59.41	58.42	50.31	53.27	61.39	55.45	56.37
		Cross-Atten	49.54	67.33	54.46	51.56	66.36	52.48	60.40	57.45
		MLP-Mixer	50.15	63.37	60.40	51.56	62.62	61.39	61.39	58.70
		Atten-Mixer(Ours)	51.69	66.34	60.40	51.88	59.81	61.39	62.38	59.13
Domain-by-Domain										
Visual (Face frames) + Visual (AU+Gaze+Affect)	Score-level	Average	54.77	46.53	59.41	50.62	57.94	59.41	58.42	55.30
		Concat	53.85	53.47	63.37	51.88	57.94	65.35	58.42	57.75
	Feature-level	SE-Concat	56.62	44.55	63.37	52.19	54.21	58.42	59.41	55.54
		Cross-Atten	54.15	49.50	62.38	54.69	57.01	60.40	63.37	57.36
		MLP-Mixer	57.54	62.38	71.29	51.25	54.21	62.38	62.38	60.20
		Atten-Mixer(Ours)	57.54	58.42	63.37	52.19	69.16	60.40	64.36	60.78
Visual (Face frames) + Audio (Mel spectrogram)	Score-level	Average	52.00	50.50	58.42	51.56	57.94	61.39	60.40	56.03
		Concat	50.46	59.41	62.38	52.19	60.75	56.44	57.43	57.01
	Feature-level	SE-Concat	55.38	48.51	58.42	52.81	62.62	57.43	59.41	56.37
		Cross-Atten	52.31	53.47	58.42	51.25	64.49	58.42	57.43	56.54
		MLP-Mixer	53.23	60.40	62.38	52.19	61.68	58.42	58.42	58.10
		Atten-Mixer(Ours)	53.85	66.34	63.37	53.75	58.88	64.36	63.37	60.56
Visual (AU+Gaze+Affect) + Audio (Mel spectrogram)	Score-level	Average	48.62	59.41	51.49	51.25	60.75	62.38	63.37	56.75
		Concat	57.23	60.40	56.44	51.25	56.07	57.43	56.44	56.47
	Feature-level	SE-Concat	55.08	60.40	59.41	54.06	60.75	61.39	57.43	58.36
		Cross-Atten	50.15	56.44	61.49	57.50	59.81	64.36	58.42	58.31
		MLP-Mixer	52.62	56.44	58.42	52.50	60.75	61.39	58.42	57.22
		Atten-Mixer(Ours)	51.69	56.44	57.43	54.06	66.36	64.36	60.40	58.68
Visual (Face frames) + Visual (AU+Gaze+Affect) + Audio (Mel spectrogram)	Score-level	Average	53.85	51.49	65.35	53.75	58.88	57.43	58.42	57.02
		Concat	52.92	52.48	55.45	53.75	62.62	62.38	56.44	56.58
	Feature-level	SE-Concat	51.38	60.40	58.42	51.56	57.01	62.38	59.41	57.22
		Cross-Atten	51.80	52.48	62.38	53.12	59.81	64.36	60.40	57.76
		MLP-Mixer	53.85	55.45	60.40	50.94	59.81	64.36	60.40	57.89
		Atten-Mixer(Ours)	55.69	61.39	59.41	55.00	58.88	59.41	60.40	58.60

dio(Mel spectrogram), “C” had Visual (AU+Gaze+Affect) + Audio (Mel spectrogram), and “D” had Visual (Face frame) + Visual (AU+Gaze+Affect) + Audio (Mel spectrogram). The results showed that models with 6 attention-mixer layers achieved the best average accuracies, followed by 7 attention-mixer layers.

4.6 Discussion

We can observe that the general performance of cross-domain deception detection is unsatisfactory because it is challenging to reduce the domain gap between each dataset.

The domain generalization ability of widely-adopted methods was relatively weak using either audio or visual features. Different domain sampling strategies worked well for different audiovisual features. Fusing multiple modalities is able to mitigate the problem. However, the performance still needs to be improved.

Ethical Consideration. Developing deception detection using AI should emphasize respecting privacy, minimizing psychological harm, preventing discrimination, promoting transparency, etc. Researchers should follow appropriate regulations to develop and deploy AI systems for

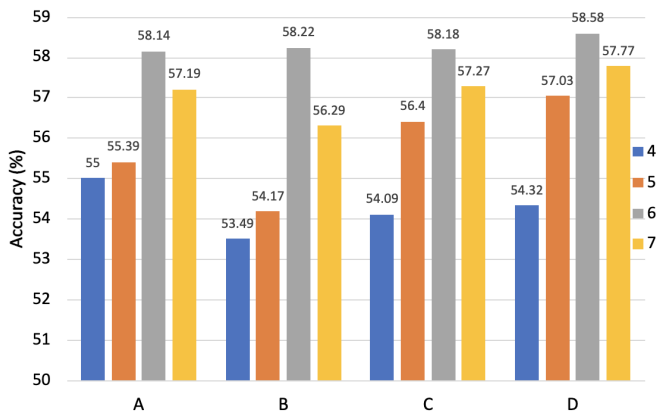


Fig. 4: Ablation study for attention-mixer layers. The number of layers 4, 5, 6, and 7 are compared. The modality and inputs for A, B, C, and D are in line with those in Table 3 from the top to the bottom.

deception detection. Potential misuses and negative impacts include invasion of privacy, discrimination, erosion of trust, etc. Mitigating these risks requires responsible practices from researchers and developers.

5 CONCLUSION

In this paper, we benchmark the cross-domain generalization performance for deception detection on publicly available datasets. We compare the single-to-single domain and multi-to-single domain generalization performances, where three strategies are used including domain-simultaneous, domain-alternating, and domain-by-domain. We also investigate the effectiveness of the gradient reversal layer for domain-simultaneous strategy. Moreover, we propose the Attention-Mixer fusion method to alleviate the domain shift issue and boost the performance. Future works for deception detection are encouraged to propose better methods to improve the domain generalizability on audio-visual deception detection task.

Acknowledgments. This work was carried out at the Rapid-Rich Object Search (ROSE) Lab, Nanyang Technological University, Singapore. The research is supported by the DSO National Laboratories, under project agreement No. DSOC21238.

REFERENCES

- [1] V. Pérez-Rosas, M. Abouelenien, R. Mihalcea, and M. Burzo, "Deception detection using real-life trial data," in *Proceedings of the 2015 ACM on International Conference on Multimodal Interaction*, 2015, pp. 59–66.
- [2] V. Gupta, M. Agarwal, M. Arora, T. Chakraborty, R. Singh, and M. Vatsa, "Bag-of-lies: A multimodal dataset for deception detection," in *Proceedings of the IEEE/CVF Conference on Computer Vision and Pattern Recognition Workshops*, 2019, pp. 0–7.
- [3] E. P. Lloyd, J. C. Deska, K. Hugenberg, A. R. McConnell, B. T. Humphrey, and J. W. Kunstman, "Miami university deception detection database," *Behavior research methods*, vol. 51, no. 1, pp. 429–439, 2019.
- [4] F. Soldner, V. Pérez-Rosas, and R. Mihalcea, "Box of lies: Multimodal deception detection in dialogues," in *Proceedings of the 2019 Conference of the North American Chapter of the Association for Computational Linguistics: Human Language Technologies, Volume 1 (Long and Short Papers)*, 2019, pp. 1768–1777.
- [5] M. Ding, A. Zhao, Z. Lu, T. Xiang, and J.-R. Wen, "Face-focused cross-stream network for deception detection in videos," in *Proceedings of the IEEE/CVF Conference on Computer Vision and Pattern Recognition*, 2019, pp. 7802–7811.
- [6] Z. Wu, B. Singh, L. Davis, and V. Subrahmanian, "Deception detection in videos," in *Proceedings of the AAAI conference on artificial intelligence*, vol. 32, no. 1, 2018.
- [7] M. Gogate, A. Adeel, and A. Hussain, "Deep learning driven multimodal fusion for automated deception detection," in *2017 IEEE symposium series on computational intelligence (SSCI)*. IEEE, 2017, pp. 1–6.
- [8] L. Mathur and M. J. Matarić, "Unsupervised audio-visual subspace alignment for high-stakes deception detection," in *ICASSP 2021-2021 IEEE International Conference on Acoustics, Speech and Signal Processing (ICASSP)*. IEEE, 2021, pp. 2255–2259.
- [9] G. Wang, H. Chen, and H. Atabakhsh, "Criminal identity deception and deception detection in law enforcement," *Group Decision and Negotiation*, vol. 13, pp. 111–127, 2004.
- [10] H. Joudaki, A. Rashidian, B. Minaei-Bidgoli, M. Mahmoodi, B. Geraili, M. Nasiri, and M. Arab, "Using data mining to detect health care fraud and abuse: a review of literature," *Global Journal of Health Science*, vol. 7, no. 1, pp. 194–202, 2014.
- [11] F. H. Glancy and S. B. Yadav, "A computational model for financial reporting fraud detection," *Decision Support Systems*, vol. 50, no. 3, pp. 595–601, 2011.
- [12] J. Synnott, D. Dietzel, and M. Ioannou, "A review of the polygraph: history, methodology and current status," *Crime Psychology Review*, vol. 1, no. 1, pp. 59–83, 2015.
- [13] S. Porter and M. Campbell, "A. vrij, detecting lies and deceit: The psychology of lying and implications for professional practice," *Expert Evidence*, vol. 7, pp. 227–232, 09 1999.
- [14] A. Nortje and C. Tredoux, "How good are we at detecting deception? a review of current techniques and theories," *South African Journal of Psychology*, vol. 49, no. 4, pp. 491–504, 2019.
- [15] H. Karimi, J. Tang, and Y. Li, "Toward end-to-end deception detection in videos," in *2018 IEEE International Conference on Big Data (Big Data)*. IEEE, 2018, pp. 1278–1283.
- [16] M. Karnati, A. Seal, A. Yazidi, and O. Krejcar, "Lienet: a deep convolution neural networks framework for detecting deception," *IEEE Transactions on Cognitive and Developmental Systems*, 2021.
- [17] D. Avola, L. Cinque, G. L. Foresti, and D. Pannone, "Automatic deception detection in rgb videos using facial action units," in *Proceedings of the 13th International Conference on Distributed Smart Cameras*, 2019, pp. 1–6.
- [18] J.-T. Yang, G.-M. Liu, and S. C.-H. Huang, "Multimodal deception detection in videos via analyzing emotional state-based feature," *arXiv preprint arXiv:2104.08373*, 2021.
- [19] I. O. Tolstikhin, N. Houlsby, A. Kolesnikov, L. Beyer, X. Zhai, T. Unterthiner, J. Yung, A. Steiner, D. Keysers, J. Uszkoreit et al., "Mlp-mixer: An all-mlp architecture for vision," *Advances in Neural Information Processing Systems*, vol. 34, pp. 24 261–24 272, 2021.
- [20] D. B. Buller and J. K. Burgoon, "Interpersonal deception theory," *Communication theory*, vol. 6, no. 3, pp. 203–242, 1996.
- [21] M. Hartwig and C. F. Bond Jr, "Why do lie-catchers fail? a lens model meta-analysis of human lie judgments," *Psychological bulletin*, vol. 137, no. 4, p. 643, 2011.
- [22] A. Vrij, *Detecting lies and deceit: The psychology of lying and implications for professional practice*. Wiley, 2000.

- [23] B. M. DePaulo, J. J. Lindsay, B. E. Malone, L. Muhlenbruck, K. Charlton, and H. Cooper, "Cues to deception." *Psychological bulletin*, vol. 129, no. 1, p. 74, 2003.
- [24] T. R. Levine and S. A. McCornack, "Theorizing about deception," *Journal of Language and Social Psychology*, vol. 33, no. 4, pp. 431–440, 2014.
- [25] A. Vrij and P. A. Granhag, "Eliciting cues to deception and truth: What matters are the questions asked," *Journal of Applied Research in Memory and Cognition*, vol. 1, no. 2, pp. 110–117, 2012.
- [26] J. B. Hirschberg, S. Benus, J. M. Brenier, F. Enos, S. Friedman, S. Gilman, C. Girand, M. Graciarena, A. Kathol, L. Michaelis *et al.*, "Distinguishing deceptive from non-deceptive speech," 2005.
- [27] G. Warren, E. Schertler, and P. Bull, "Detecting deception from emotional and unemotional cues," *Journal of Nonverbal Behavior*, vol. 33, no. 1, pp. 59–69, 2009.
- [28] P. Ekman and W. V. Friesen, "Nonverbal leakage and clues to deception," *Psychiatry*, vol. 32, no. 1, pp. 88–106, 1969.
- [29] —, "Detecting deception from the body or face." *Journal of personality and Social Psychology*, vol. 29, no. 3, p. 288, 1974.
- [30] L. Mathur and M. J. Matarić, "Introducing representations of facial affect in automated multimodal deception detection," in *Proceedings of the 2020 International Conference on Multimodal Interaction*, 2020, pp. 305–314.
- [31] K. He, X. Zhang, S. Ren, and J. Sun, "Deep residual learning for image recognition," in *IEEE conference on computer vision and pattern recognition*, 2016, pp. 770–778.
- [32] B. Amos, B. Ludwiczuk, M. Satyanarayanan *et al.*, "Openface: A general-purpose face recognition library with mobile applications," *CMU School of Computer Science*, vol. 6, no. 2, p. 20, 2016.
- [33] A. Toisoul, J. Kossaifi, A. Bulat, G. Tzimiropoulos, and M. Pantic, "Estimation of continuous valence and arousal levels from faces in naturalistic conditions," *Nature Machine Intelligence*, vol. 3, no. 1, pp. 42–50, 2021.
- [34] F. Eyben, M. Wöllmer, and B. Schuller, "Opensmile: the munich versatile and fast open-source audio feature extractor," in *Proceedings of the 18th ACM international conference on Multimedia*, 2010, pp. 1459–1462.
- [35] Z. Wang, Z. Wang, Z. Yu, W. Deng, J. Li, T. Gao, and Z. Wang, "Domain generalization via shuffled style assembly for face anti-spoofing," in *Proceedings of the IEEE/CVF Conference on Computer Vision and Pattern Recognition*, 2022, pp. 4123–4133.
- [36] T. Varanka, Y. Li, W. Peng, and G. Zhao, "Data leakage and evaluation issues in micro-expression analysis," *IEEE Transactions on Affective Computing*, 2023.
- [37] A. Vaswani, N. Shazeer, N. Parmar, J. Uszkoreit, L. Jones, A. N. Gomez, Ł. Kaiser, and I. Polosukhin, "Attention is all you need," *Advances in neural information processing systems*, vol. 30, 2017.
- [38] H. U. D. Ahmed, U. I. Bajwa, F. Zhang, and M. W. Anwar, "Deception detection in videos using the facial action coding system," *arXiv preprint arXiv:2105.13659*, 2021.
- [39] K. Zhang, Z. Zhang, Z. Li, and Y. Qiao, "Joint face detection and alignment using multitask cascaded convolutional networks," *IEEE Signal Processing Letters*, vol. 23, no. 10, pp. 1499–1503, 2016.
- [40] J. Chung, C. Gulcehre, K. Cho, and Y. Bengio, "Empirical evaluation of gated recurrent neural networks on sequence modeling," *arXiv preprint arXiv:1412.3555*, 2014.
- [41] L. Noriega, "Multilayer perceptron tutorial," *School of Computing. Staffordshire University*, vol. 4, no. 5, p. 444, 2005.
- [42] A. Baevski, Y. Zhou, A. Mohamed, and M. Auli, "wav2vec 2.0: A framework for self-supervised learning of speech representations," *Advances in Neural Information Processing Systems*, vol. 33, pp. 12 449–12 460, 2020.
- [43] Y. Ganin and V. Lempitsky, "Unsupervised domain adaptation by backpropagation," in *International conference on machine learning*. PMLR, 2015, pp. 1180–1189.
- [44] J. Hu, L. Shen, and G. Sun, "Squeeze-and-excitation networks," in *Proceedings of the IEEE conference on computer vision and pattern recognition*, 2018, pp. 7132–7141.